Article:
Wilson, M.C.T., Gaskell, P.H. and Savage, M.D. (2001) Flow in a double-film-fed fluid bead between contra-rotating rolls, Part 1: equilibrium flow structure. European Journal of Applied Mathematics, 12 (3). pp. 395-411. ISSN: 0956-7925

https://doi.org/10.1017/S0956792501004399

Euro. Jnl of Applied Mathematics (2001), *vol.* 12, *pp.* 395–411. Printed in the United Kingdom

Flow in a double-film-fed fluid bead between contra-rotating rolls Part 1: equilibrium flow structure

M. C. T. WILSON[1], P. H. GASKELL[1] and M. D. SAVAGE[2]

[1] *School of Mechanical Engineering, University of Leeds, Leeds LS2 9JT, UK*
[2] *Department of Physics and Astronomy, University of Leeds, Leeds LS2 9JT, UK*

(*Received 22 September 1999; revised 30 September 2000*)

In multiple-roll coaters thin liquid films are transferred from roll to roll by means of liquid 'beads' which occupy the small gaps between adjacent rolls. Double-Film-Fed (DFF) beads are those which feature *two* ingoing films instead of the usual one, and arise in the intermediate stages of certain types of roll coater. One of the ingoing films, h_1, is supplied from the previous inter-roll gap while the other, h_2, 'returns' from the subsequent gap. Such a flow is investigated here under the conditions of low flow rate, small capillary number and negligible gravity and inertia, using lubrication theory and finite element analysis. The thickness of film h_1 is fixed independently, while that of h_2 is specified as a fraction, ζ, of the film output on the same roll. This simple approach allows a degree of feedback between the output and input of the bead, and enables one to simulate different conditions in the subsequent gap. Predictions of outgoing film thicknesses made using the two models agree extremely well and show that, for each value of $\zeta < 1$, one outgoing film thickness decreases monotonically with speed ratio, S, while the other features a maximum. Good agreement is also seen in the pressure profiles, which are entirely sub-ambient in keeping with the small capillary number conditions. The finite element solutions reveal that in the 'zero-flux' case (when $\zeta = 1$) the flow structures are very similar to those seen in an idealized cavity problem. In the more general ($\zeta < 1$) situation, as in single-film-fed meniscus roll coating, several liquid transfer-jets occur by which liquid is conveyed through the bead from one roll to the other. The lubrication model is used to calculate several critical flow rates at which the flow is transformed, and it is shown that when the total dimensionless flow rate through the bead exceeds 1/3, the downstream flow structure is independent of the relative sizes of the ingoing films.

1 Introduction

Roll coating is a versatile industrial process used to deposit a thin, uniform liquid film on to a substrate (or 'web') such as paper, metal or plastic. Figure 1 shows a simple three-roll coater operating in 'forward' mode (meaning that roll surfaces pass through the small inter-roll gaps in the same direction). Viscous lifting provides the mechanism by which coating liquid is drawn from the reservoir, and under stable operating conditions two liquid 'beads' exist in the inter-roll gaps. As can be seen in Figure 1, the only difference between the beads is the number of liquid films supplying them: the upper bead, through

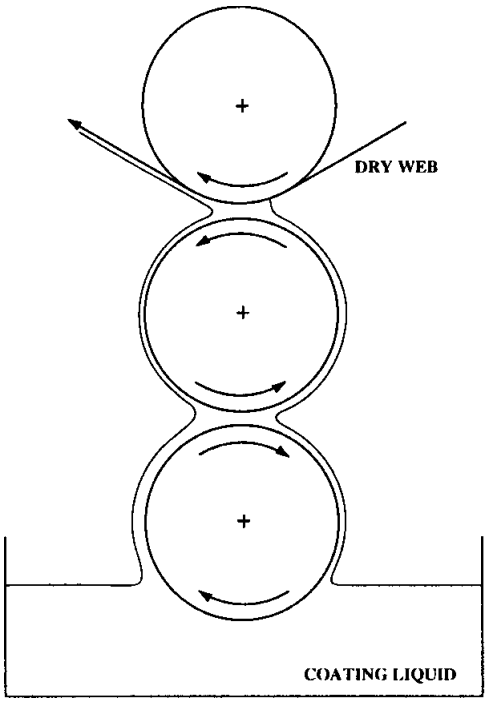

FIGURE 1. A simple three-roll forward roll coater.

which the dry substrate passes, is said to be Single-Film-Fed (SFF) while the lower bead is Double-Film-Fed (DFF).

There is a wealth of literature on the flow in individual SFF forward roll coating gaps – for a comprehensive review, see Coyle [5] – and one of the most important results from these works is an understanding of how the film-split ratio depends on operating conditions. Generally, an expression of the form

$$\frac{h_3}{h_4} = \alpha S^{\beta} \tag{1.1}$$

is found, where h_3 and h_4 are the two outgoing film thicknesses (see later), S is the speed ratio of the rolls, and α and β are functions of other operating parameters. Once the behaviour of an individual gap flow is understood, one can construct a model for a multiple-roll coater by equating the output of one gap to the input of the next [2].

In contrast to the SFF flow, there are few studies which consider the DFF case. This is perhaps not surprising since, though the flux through the nip is different, the film-splitting behaviour (equation 1.1) is the same. The presence of the returning film does, however, have implications for the structure of the flow and – more importantly – its stability to 'bead break'. The present paper focuses on the structure of the DFF fluid bead, while Part 2 addresses the issue of stability.

Benjamin [1] used lubrication theory to model the DFF flow. He imposed both ingoing film thicknesses in terms of the total flux through the nip and an inlet film thickness ratio. On the downstream side he assumed that the film-split occurred at the first stagnation point in the flow and that this point lay on the free surface. Applying the 'Prandtl-

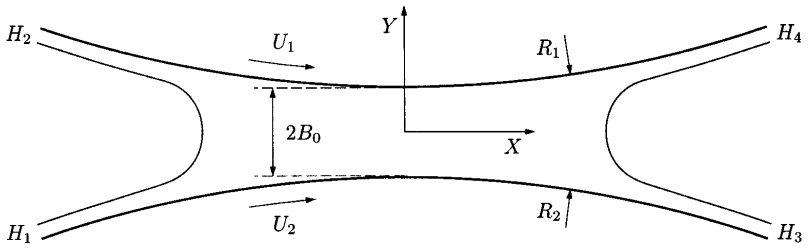

FIGURE 2. The double-film-fed forward roll coating gap.

Hopkins' conditions for separation [3] then gave the downstream meniscus location. With the menisci approximated as circular arcs to account for capillary pressure, the lubrication equations could be solved for the upstream 'film-merge' location.

Predictions of the pressure profile made using the above model were tested against those from a Finite Element (FE) analysis of the complete domain, and a discrepancy was found due to the assumption that the film splits at the meniscus. In fact there is usually a region of recirculating flow and the first stagnation point lies further upstream [6]. The FE solutions were also used to investigate the flow structure in the film-merge region close to the upstream free surface, and showed that recirculations grew as flow rate increased, until the flow became unsteady and three-dimensional when the flux passed a critical value. The structure of the flow in the rest of the domain was not considered.

In the next section a lubrication theory model is developed which is valid for small capillary numbers and low flow rates. It is used in conjunction with the FE formulation outlined in § 3 to explore the effect of the returning film on the flow structure throughout the DFF fluid bead.

2 Lubrication theory model

Figure 2 shows the domain of interest, namely the gap between a pair of counter-rotating rolls featuring four liquid films, $H_1, \ldots, H_4$. Film H_1 is taken to be the inlet film (i.e. that supplied from the reservoir) and is a specified parameter. If the gap in Figure 2 is considered to be part of a multiple-roll coater, then the thickness of the other ingoing film, H_2, will depend on the nature of the flow in the subsequent gap and on the thickness of film H_4 (see Figure 1). As mentioned above, Benjamin [1] chose to impose the thicknesses of films H_1 and H_2 by specifying the ratio H_2/H_1 and a total flow rate. Here H_1 is fixed independently and H_2 is imposed as a fraction of H_4, i.e.

$$H_2 = \zeta H_4, \tag{2.1}$$

where $0 \leqslant \zeta \leqslant 1$. Thus when $\zeta = 0$ film H_2, referred to as the 'returning' film, is absent whereas $\zeta = 1$ implies that there is no net fluid transfer from one roll to the other. This approach, though simple, allows for a degree of 'feedback' between the output and the input of the system, and hence allows one to simulate various conditions in the subsequent gap.

For simplicity, the rolls are assumed to have equal radii, i.e. $R_1 = R_2 = R$. The effects of gravity and inertia are taken to be negligible, and the liquid is considered to be Newtonian

with viscosity μ and constant surface tension σ. The gap between the rolls is typically much smaller than their radii (i.e. $\delta \equiv \sqrt{B_0/2R} \ll 1$) and the appropriate dimensionless scheme is well-established [6]:

$$x = \frac{X}{\sqrt{2RB_0}}; \quad y = \frac{Y}{B_0}; \quad u = \frac{U}{U_2}; \quad p = \frac{PB_0}{\mu U_2}\left(\frac{B_0}{2R}\right)^{\frac{1}{2}}; \quad q = \frac{Q}{2U_2B_0} \tag{2.2}$$

where u is the horizontal velocity component and q is the dimensionless flow rate through the nip. The governing equations reduce to Reynolds equation for the pressure, p:

$$\frac{dp}{dx} = \frac{3(1+S)(1+x^2) - 6q}{2(1+x^2)^3}. \tag{2.3}$$

Using the substitution $x = \tan\theta$ gives the solution

$$p = \tfrac{3}{4}(1 + S - 2q)(\theta + \tfrac{1}{2}\sin 2\theta) + \tfrac{3}{8}q(\theta - \tfrac{1}{4}\sin 4\theta) + C, \tag{2.4}$$

where C is a constant of integration. Two boundary conditions on p are required. The domain of validity of (2.3), $-x_u^* \leqslant x \leqslant x_d^*$, does not extend quite as far as the menisci, but it is assumed that $-x_u^*$ and x_d^* lie sufficiently close to their respective menisci that the pressure at each end point can be taken as the capillary pressure at the appropriate meniscus. Measuring pressures relative to the ambient pressure, the balance of stresses at each free surface gives the following two conditions

$$p(\theta = -\theta_u) = -\frac{\delta}{r_u Ca}, \qquad p(\theta = \theta_d) = -\frac{\delta}{r_d Ca}, \tag{2.5}$$

where $Ca = \mu U_2/\sigma \sim O(\delta)$ is the capillary number, r_u $(= R_u/B_0)$ and r_d $(= R_d/B_0)$ are the dimensionless radii of curvature of the upstream and downstream menisci, respectively, $\theta_u = \tan^{-1} x_u$, and $\theta_d = \tan^{-1} x_d$. Applying these conditions to (2.4) yields

$$\begin{aligned}\frac{2\delta}{3Ca}\left[\frac{1}{r_u} - \frac{1}{r_d}\right] &= (S+1)\left[\tfrac{1}{2}(\theta_u + \theta_d) + \tfrac{1}{4}(\sin 2\theta_u + \sin 2\theta_d)\right] \\ &\quad - q\left[\tfrac{3}{4}(\theta_u + \theta_d) + \tfrac{1}{2}(\sin 2\theta_u + \sin 2\theta_d) + \tfrac{1}{16}(\sin 4\theta_u + \sin 4\theta_d)\right].\end{aligned} \tag{2.6}$$

To proceed, r_u, r_d must be expressed in terms of θ_u and θ_d. This can be achieved in a simple way by approximating the menisci as arcs of circles whose radii are equal to half the local gap between the rolls. Since the semi-gap is approximated by a parabola [6], this gives

$$r_u = \sec^2\theta_u, \quad r_d = \sec^2\theta_d. \tag{2.7 a,b}$$

Note that better approximations for r_u and r_d can be made by subtracting the film thicknesses from the local gap or accounting for the divergence of the roll surfaces [14]. For the purposes of the present paper, however, the simple approximation (2.7) is quite adequate. Improvements to the lubrication model are discussed in Part 2.

In fact, it is possible to determine x_d without solving (2.6). Assuming plug flow in each film, the balance of fluxes upstream and downstream takes the form

$$h_1 + Sh_2 = h_3 + Sh_4, \tag{2.8}$$

where $h_i = H_i/B_0$, $i = 1, \ldots, 4$ are the dimensionless film thicknesses. For small capillary

number, at leading order the films h_3 and h_4 are related to r_d by [4,13]:

$$h_3 = r_d \alpha Ca^{2/3}, \quad h_4 = r_d \alpha (SCa)^{2/3}, \tag{2.9 a,b}$$

where $\alpha = 1.337$. Again only the leading order expressions are used here; higher order effects are considered in detail in Part 2. At the upstream the film thicknesses are

$$h_1 = 2\lambda, \quad h_2 = \zeta h_4. \tag{2.10 a,b}$$

Using (2.7), (2.9) and (2.10), equation (2.8) yields

$$x_d^2 = \frac{2\lambda}{\alpha Ca^{2/3}(1 + (1-\zeta)S^{5/3})} - 1. \tag{2.11}$$

Hence, the outgoing film thicknesses are

$$h_3 = \frac{2\lambda}{1 + (1-\zeta)S^{5/3}}, \quad h_4 = \frac{2\lambda S^{2/3}}{1 + (1-\zeta)S^{5/3}}, \tag{2.12 a,b}$$

and the dimensionless flux through the nip, $q = \frac{1}{2}(h_1 + Sh_2) = \frac{1}{2}(h_3 + Sh_4)$, is

$$q = \frac{\lambda(1 + S^{5/3})}{1 + (1-\zeta)S^{5/3}}. \tag{2.13}$$

Now (2.6) can be solved numerically for the upstream meniscus location, x_u.

3 Finite element formulation

The above lubrication model can provide much information about the pressure in the bead and the film thicknesses, and it can also be used to predict critical flow rates at which flow structures change [10]. However, to infer two-dimensional flow structures from one-dimensional lubrication theory first requires a knowledge of what features to look for. For a more complete picture of the flow and to explore a wider range of parameters one must turn to a numerical solution. The most popular method used to model coating flows is arguably the Finite Element (FE) method, and that is the technique employed here.

Since roll coating flows are generally characterized by low Reynolds numbers, the Stokes equations were taken as the governing equations and were solved using a Galerkin weighted residual formulation. The usual boundary conditions were applied: no-slip on the roll surfaces; zero shear stress, zero normal velocity, and surface tension balanced with normal stress on the free surfaces; and plug flow in the films. Following Benjamin [1], the pressure datum was set by fixing p in the films to be equal to the capillary pressure due to the (positive) curvature of the rolls:

$$p = \frac{1}{Ca}\left(\frac{H_0}{R}\right). \tag{3.1}$$

Note that the ambient pressure is assumed to be zero and the film thicknesses have been neglected since they are small compared to R. This allows (3.1) to be imposed as an essential condition on the inflow and outflow planes.

The domain was tessellated into triangular 'V6/P3' elements, and the free surfaces were parametrized by the 'spine method' [12]. The construction of the mesh followed that used

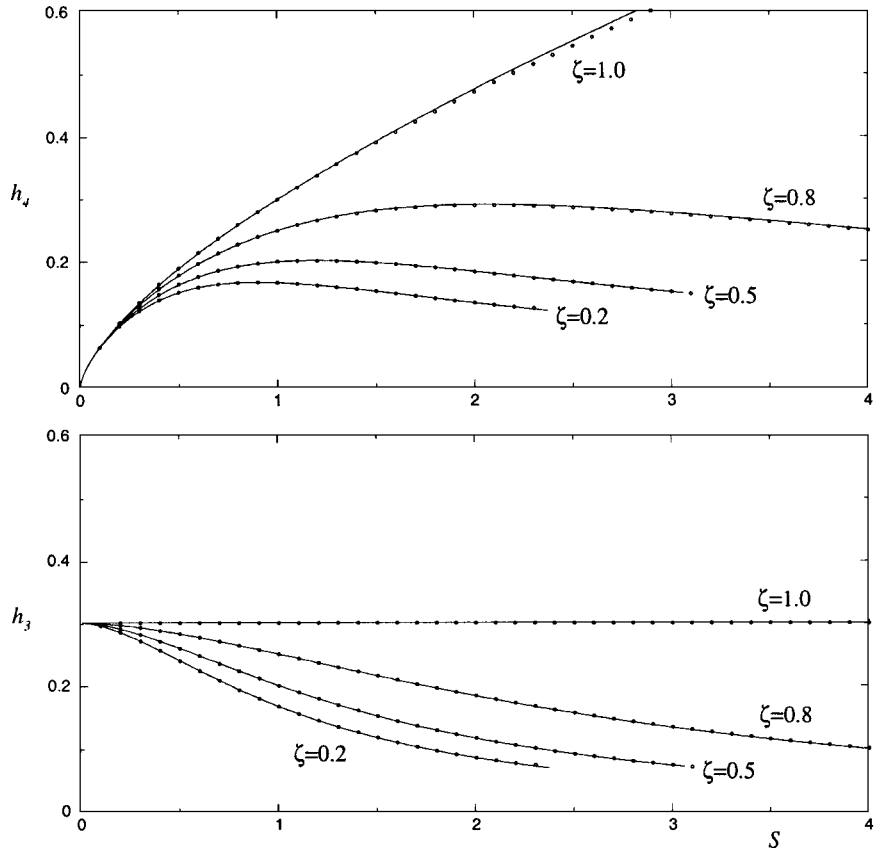

FIGURE 3. Variation of outgoing film thicknesses with S for various values of ζ. Curves: lubrication theory; points: FE analysis. Other parameters: $\lambda = 0.15$, $Ca = 0.01$, $B_0/R = 0.01$.

by Coyle *et al.* [6] in forward roll coating – see Wilson [16] for more specific details. The residual equations were solved by Newton iteration in which the Jacobian was inverted using the frontal method [11], and the iterative process was terminated when the largest increment to the solution was less than 10^{-6}.

4 Results and discussion

4.1 Film thicknesses

Figure 3 is a typical plot of the variation of film thicknesses h_3 and h_4 with S calculated from (2.12) and by finite element analysis. Excellent agreement exists between the two sets of results; only at high S and ζ does a discernible difference appear in the predictions of h_4. When $\zeta = 1$ there is no net transfer of liquid from one roll to the other, so film h_3 is always equal to 2λ (i.e. 0.3 in this case). Film h_4, on the other hand, increases as $S^{2/3}$ in accordance with (2.12*b*). For $\zeta < 1$, the curves for each film look similar: h_4 reaches a maximum which occurs at a higher S as ζ increases, while h_3 decreases monotonically with S. The $\zeta = 0.2$ and 0.5 curves terminate at the value of S for which $x_u = x_d$, i.e.

the two menisci coincide. Describing the flow in the bead when the menisci are close together is difficult both analytically and numerically. In the case of the former, the higher order terms ignored here start to play an important role (see Part 2), whereas in the finite element formulation meshing problems are encountered. In the remainder of this paper, only conditions for which the two menisci are well-separated will be considered.

4.2 Flow structures: zero net flux case

In inlet-flooded forward roll coating there are generally three streamline topologies associated with the film-splitting flow: a simple film-split with no recirculations, one with two 'joint eddies' both connected to the free surface and to each other, and another featuring 'disjoint eddies' where only one eddy attaches to the free surface [15]. Since in the current problem the upstream half of the domain is topologically equivalent to the downstream, flow structures similar to the above also arise in the 'film-merge' region. However, at small flow rates, when the menisci lie closer together, the essentially independent upstream and downstream flow structures are replaced by full-bead structures resembling cavity flows [8, 10]. Below, the parametric response of the DFF bead is described by means of a few examples. A more detailed discussion of similar flow structures in the SFF bead is in preparation [14].

When $\zeta = 1$ the thickness of the returning film is the same as that carried out of the bead by the upper roll. Consequently there is no net flux of liquid from one roll to the other. Obviously, such an arrangement would not occur in practice as the purpose of a roll coater is to transfer liquid from a source to a web. The zero flux case is interesting theoretically, however, and has been used in experiments to measure meniscus shapes [7].

4.2.1 *Symmetric flow*

The first case considered is that of a small inlet flux, λ, and equal roll speeds, $S = 1$. Figure 4 shows the flow structures seen at different inlet flow rates. When λ is small, the flow in the bead features two equal recirculations defined by three separating streamlines stretching across the entire width of the bead. Each recirculation contains a saddle point and two centres, Figure 4(*a*), and the flow is very similar to that observed in 'meniscus roll coating' [10] and the idealized rectangular cavity model of that flow [8]. As λ increases, the liquid layers on each roll thicken and push the separating streamlines closer together until at a critical flow rate ($\lambda \approx 0.1662$) the saddle points in the recirculations coalesce and all three separating streamlines connect together, Figure 4(*b*). A further increase in λ results in the two saddles moving apart along $y = 0$ (Figure 4*c*), however they remain connected to each other and also to one of the free surfaces.

A similar transformation of the flow structure was seen by Gaskell *et al.* [10] in the Single-Film-Fed (SFF) forward roll coater, except that the upstream saddle point does not connect to the upstream free surface since liquid must be transferred from the bottom roll to the top. They found that for $S = 1$ the critical flow rate at which the saddle points coalesce was $\lambda \approx 0.3327$. To compare with the present problem, one must consider the flux passing through the nip; in the SFF case, this is equal to λ whereas in the present problem the flux in the returning film must be added. When $S = \zeta = 1$ all four films

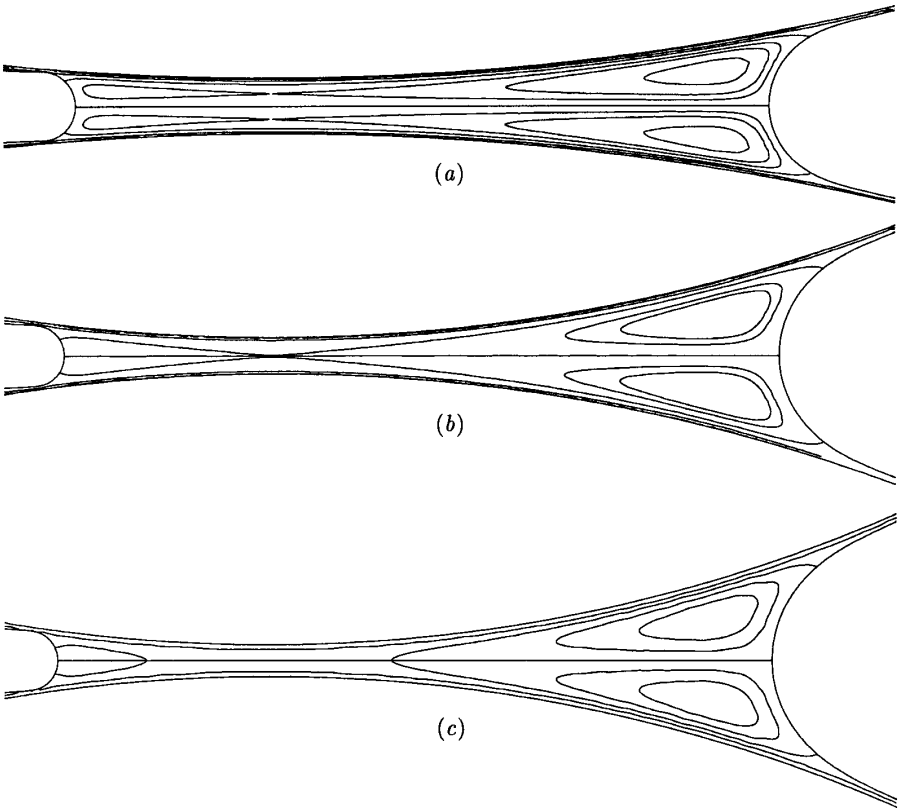

FIGURE 4. Effect of increasing inlet flux on flow structure. (*a*) $\lambda = 0.08$: three separating streamlines define two closed regions each of which contains a saddle point and two sub-eddies; (*b*) $\lambda = 0.1662$: all three separating streamlines connect as the two saddle points coalesce; (*c*) $\lambda = 0.21$: the two interior saddle points move apart, but remain connected to each other and to the six separation points. Other parameters: $Ca = 0.01$, $S = 1$, $B_0/R = 0.01$, $\zeta = 1$.

have the same thickness, and so the critical flux through the nip is $2\lambda \approx 0.3324$, which compares well with the value quoted above.

The critical flow rate at which the separating streamlines connect can be predicted using lubrication theory. The streamfunction at any point on $x = 0$ is given by

$$\begin{aligned}\psi(0, y) &= \int_{-1}^{y} u(0, \tau) d\tau \\ &= \tfrac{3}{8}(S + 1 - 2q)(\tfrac{1}{3}y^3 - y - \tfrac{2}{3}) + \tfrac{1}{8}(S - 1)(y^2 - 1) + \tfrac{1}{4}(S + 1)(y + 1),\end{aligned} \tag{4.1}$$

where $\psi(0, -1) = 0$ has been used to fix the arbitrary constant. The positions of the separating streamlines can then be found by solving

$$\psi(0, y) - \lambda = 0 \tag{4.2}$$

for y. When $\zeta = 1$ and $S = 1$, q is equal to 2λ and the equation for y is thus

$$y[(1 - 2\lambda)y^2 - (1 - 6\lambda)] = 0. \tag{4.3}$$

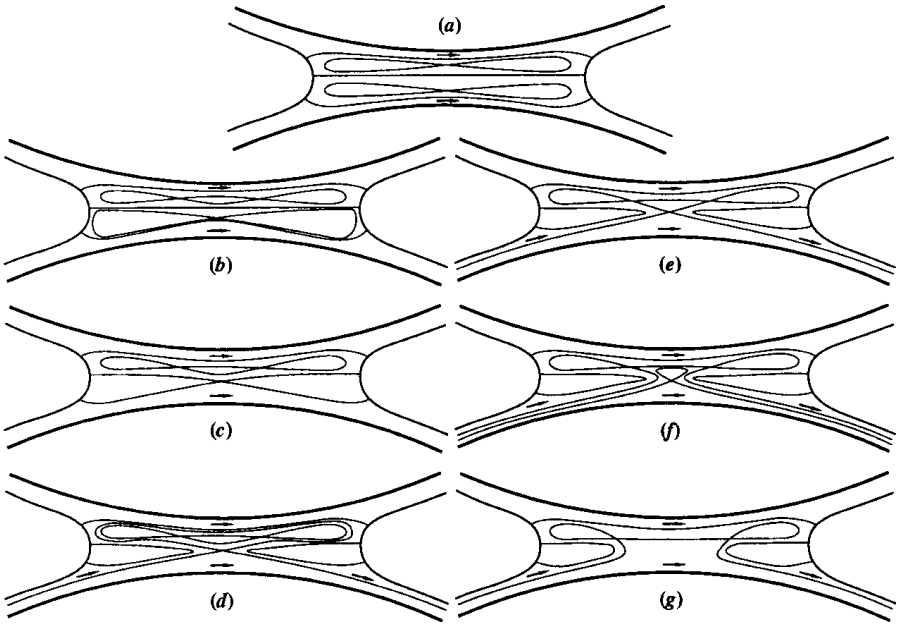

FIGURE 5. The effect of increasing λ on flow structure at $\zeta = 1$ and $S < 1$.

The solutions are

$$y_1 = 0 \quad \text{and} \quad y_{2,3} = \pm\sqrt{\frac{1-6\lambda}{1-2\lambda}}, \tag{4.4}$$

and hence it follows that the separating streamlines will coalesce at $\lambda = \frac{1}{6}$ which compares well with the FE calculation of 0.1662.

4.2.2 *Asymmetric flow*

The sequence of transformations arising when λ is increased and $S < 1$ is shown in Figure 5 which gives schematic representations of the flow based on the magnified views of FE solutions given in Figure 6. When $\lambda = 0.19$ the flow structure (Figure 5*a*) is the same as in Figure 4(*a*) but the lower recirculation is rather larger than the upper since the lower roll surface is moving faster. As λ increases, the separating streamlines again move together but at a critical flow rate the saddle point in the upper recirculation becomes a centre and the double-eddy structure is transformed into the treble-eddy structure, Figure 5*b*, seen in the idealized cavity problem [8].

As the flux continues to increase, the lower separating streamlines connect at the lower saddle point which remains on $x = 0$ (Figure 5*c*). This structure exists only for one particular λ; at higher values the separating streamlines separate from and reattach to the same free surface and no longer span the width of the bead. A consequence of this is that the liquid entering the bead on the bottom roll is divided such that some passes directly through the nip on the lower roll while the rest travels around the various eddies in the bead and then returns to the lower roll before exiting, see Figures 5(*d*) and 6(*b*).

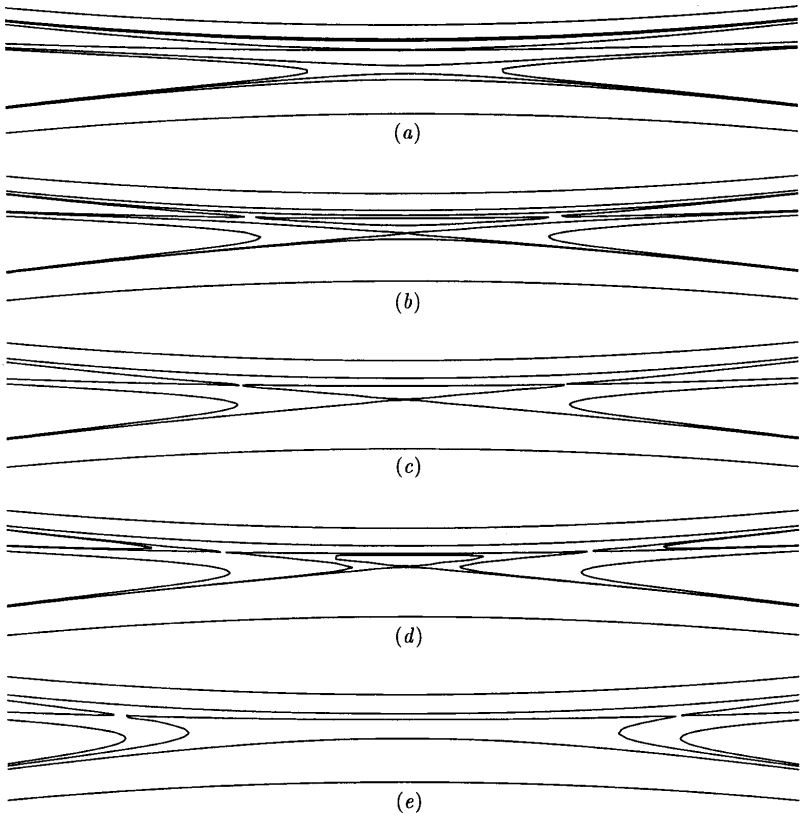

FIGURE 6. Close-up views of the important streamlines illustrating the effect of increasing λ on flow structure at $S = 0.4$ and $\zeta = 1$. (*a*) $\lambda = 0.19$; (*b*) $\lambda = 0.202$; (*c*) $\lambda = 0.2054$; (*d*) $\lambda = 0.206$; (*e*) $\lambda = 0.23$. Other parameters: $Ca = 0.01$, $B_0/R = 0.01$.

At this stage the *dividing* streamline, (i.e. that passing through the saddle point) encloses the separatix of the treble-eddy structure as shown in Figure 5(*d*) but as λ increases these two streamlines approach each other and the next change in structure occurs when they coincide and connect together the three interior saddle points, as seen in Figures 5(*e*) and 6(*c*). Again, this is a structure which only occurs at one value of λ (for a given S) and an increase in λ results in the bottom saddle point disconnecting from the others. This gives rise to two dividing streamlines and three routes through the bead for liquid entering on the lower roll – see Figures 5(*f*) and 6(*d*). Finally, as λ increases further, the small eddy above the bottom saddle point diminishes and disappears to leave the structure in Figures 5(*g*) and 6(*e*). Note the presence of the 'disjoint eddies' mentioned earlier near each free surface. When $S > 1$ a similar transformation of the flow occurs, but all the structures involved are inverted, i.e. the 3-eddy structure arises in the lower recirculation, and so on. As a matter of interest, the sequence of flow transformations just described has been observed before in a rectangular *rigid-walled* cavity driven by the parallel and independent motion of its top and bottom plates [9]. In that problem the varied parameter was the aspect ratio of the cavity.

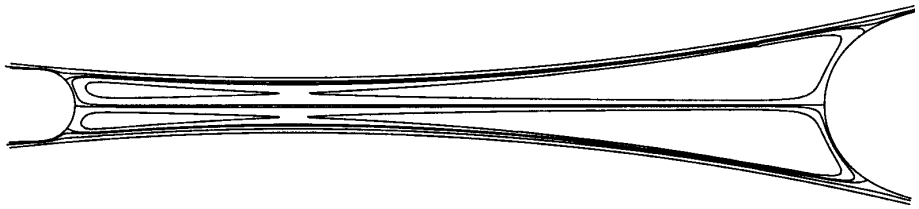

FIGURE 7. Streamlines for $S = 1$, $\zeta = 0.9$, $\lambda = 0.1$, $Ca = 0.01$, and $R/B_0 = 100$: liquid is transferred from the lower to the upper roll via a transfer-jet snaking around both the two large eddies.

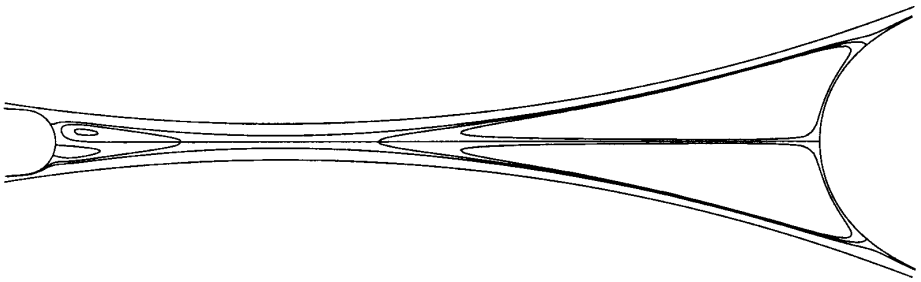

FIGURE 8. Streamlines for $S = 1$, $\zeta = 0.9$, $\lambda = 0.21$, $Ca = 0.01$, and $R/B_0 = 100$: liquid is transferred via a transfer-jet close to the upstream free surface.

4.3 Flow structures: general case

When $\zeta < 1$ the upper roll drags away more liquid than it supplies and so there must be a transfer of liquid from the lower inlet to the upper outlet. From the discussion in the previous section, it is expected that there will be a number of 'routes' by which the required amount of liquid can be transferred. It has been seen that the key factors in determining the flow structure are the thicknesses of the liquid layers on each roll and ζ is another parameter which has a pronounced effect on these thicknesses. Hence the introduction of ζ as a varying quantity combined with S and λ makes the exploration of the flow structure more difficult. For convenience the discussion is broken down into two cases.

4.3.1 *The equal speed case, $S = 1$*

When $S = 1$ there are three regimes to consider, depending on the value of λ. For $\lambda < \frac{1}{6}$ the flow in the bead consists of two large recirculations, each containing a saddle point and two centres (see Figure 4). As ζ is reduced from unity two of the separating streamlines cease to connect the free surfaces and instead separate from and reattach to the same free surface, as shown by the solution in figure 7. The double-eddy structures still exist and reside inside the recirculations defined by the separating streamlines. The liquid which must now be supplied to the upper roll is done so by means of a long transfer-jet winding between the separating streamlines. In SFF meniscus roll coating, this mechanism of transfer was referred to as the 'primary transfer-jet' [10].

On the other hand, if $\lambda > \frac{1}{6}$ the bead contains a section of unidirectional flow which remains as ζ decreases from unity; the liquid required by the upper roll is transferred via

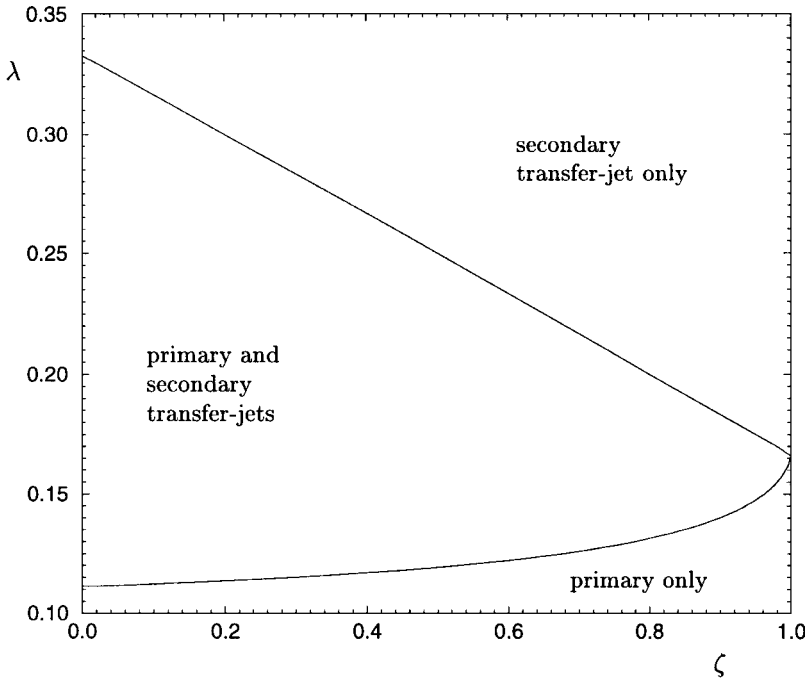

FIGURE 9. Critical flow rates as a function of ζ for $S = 1$, $Ca = 0.01$, and $B_0/R = 0.01$.

a short ('secondary' [10]) transfer-jet which passes between the dividing streamline and the upstream free surface, see figure 8.

At values of λ between those in Figures 7 and 8 it is expected that both mechanisms of flow transfer will arise. In fact, the development of the flow with λ at $S = 1$ has already been explored in the SFF forward roll coater [10]. The flow structures arising in the present problem will be the same as in the SFF case, since the point at which the topmost separating streamline separates from the upstream free surface is (topologically) similar to the dynamic contact line featured in the SFF domain. The streamline separating from that point can be considered as the effective roll surface, and so the flow will be transformed in exactly the same way as described by Gaskell *et al.* [10]. The only difference here is that the flux through the nip is not simply equal to that supplied by the lower roll, but depends on the returning film thickness also. Hence ζ will affect the values of λ at which transformations occur.

The critical events which mark the appearance and disappearance of the jets occur when one or more of the saddle points become connected to one of the free surfaces. Monitoring the positions and streamfunction values of the saddle points as ζ and λ are varied therefore yields a control space diagram as shown in Figure 9. From the graph one can see that the primary transfer-jet disappears at combinations of λ and ζ satisfying $\lambda = \frac{1}{6}(2 - \zeta)$ and since when $S = 1$

$$q = \frac{2\lambda}{2 - \zeta}, \tag{4.5}$$

this means that the total flux through the nip is always $\frac{1}{3}$ when the primary transfer-jet

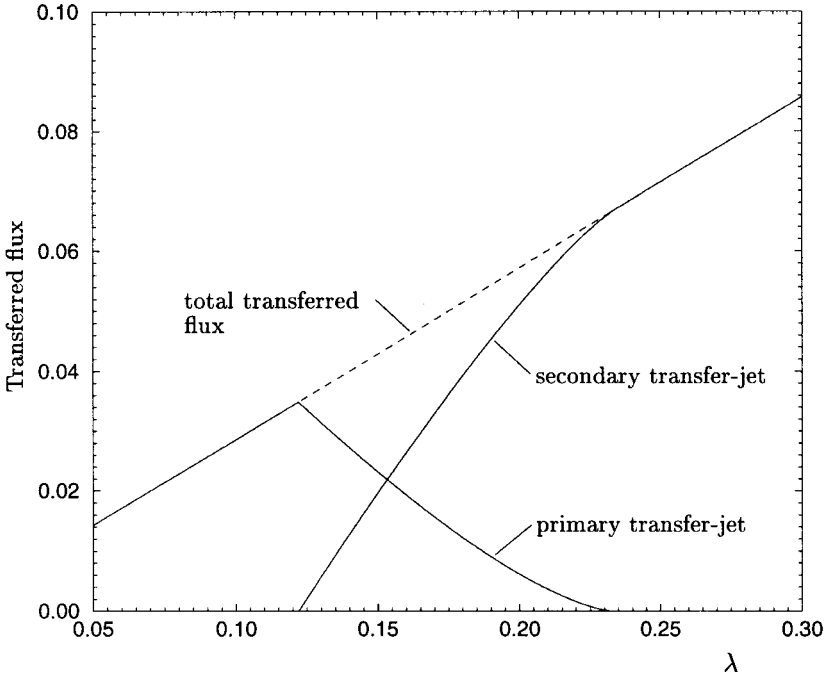

FIGURE 10. Variation of jet strengths with λ for $\zeta = 0.6$, $S = 1$, $Ca = 0.01$, and $B_0/R = 0.01$.

disappears. This critical flow rate therefore marks the transition from a bead flow where the upstream and downstream interact to a regime where the flow downstream of the nip is independent of the way in which liquid is supplied to the bead and is governed only by the total flux through the nip and the speed ratio of the rolls. In other words this is the transition from the 'meniscus' to the 'moderately-starved' regime [10].

The above result could have been predicted directly from the positions of the stagnation points on $x = 0$. From the velocity distribution associated with (2.3) it follows that these lie at

$$y_{1,2} = \frac{1 - S \pm 2\sqrt{S^2 + S + 1 - 3q(2(1+S) - 3q)}}{3(1 + S - 2q)}, \tag{4.6}$$

and the critical flow rate occurs when the discriminant is zero. This gives a quadratic for q with solutions

$$q_{1,2} = \tfrac{1}{3}(1 + S) \pm \tfrac{1}{3}\sqrt{S}. \tag{4.7}$$

When $S = 1$ the solutions are $\frac{1}{3}$ and 1, but the solution $q = 1$ can be discarded since for $S = q = 1$ the denominator in (4.6) is zero. Hence the critical flow rate is $\frac{1}{3}$.

The appearance/disappearance of the secondary jet at small λ does not occur at a constant q. As $\zeta \to 0$ the critical flow rate tends to $\frac{1}{9}$ which was calculated by Gaskell *et al.* [10], while as $\zeta \to 1$ the two curves in figure 9 approach each other since at $\zeta = 1$ there is only one critical flow rate, $\lambda = \frac{1}{6}$ ($q = \frac{1}{3}$), see Figure 4. Note that the strengths of the two transfer-jets can be calculated from the value of λ and the values of ψ at the saddle points, and their variation with λ is shown in Figure 10.

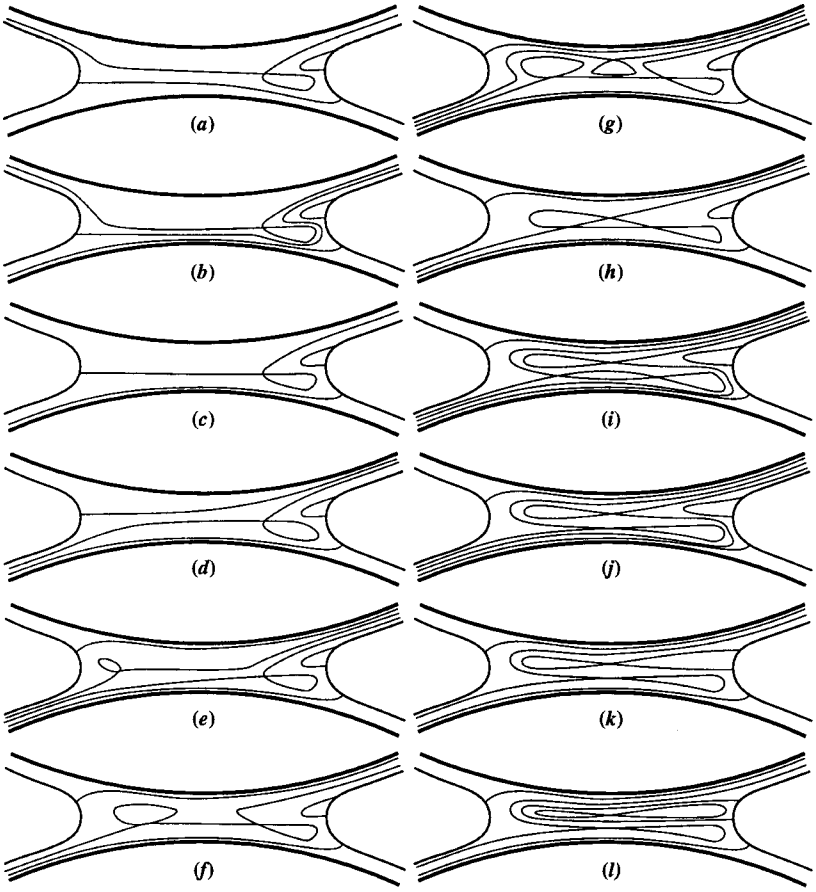

FIGURE 11. The effect of decreasing ζ on flow structure at $S = 2$, $\lambda = 0.25$, $Ca = 0.01$ and $B_0/R = 0.01$.

4.3.2 *The case of a faster upper roll, $S > 1$*

When $S \neq 1$, the transformation of the flow structure is more complicated and is illustrated here for a speed ratio of $S = 2$ by reducing the value of ζ. In the interests of brevity and clarity, only schematics are presented; supporting numerical solutions can be found elsewhere [14, 16].

When $S = 2$, $\lambda = 0.25$ and $\zeta = 1$, as in Figure 11(a), the flux through the nip is relatively large ($q = 1.03$) and the upstream eddies seen earlier are not present. Instead there is a single streamline separating from the upstream free surface which also connects to the downstream meniscus. In the downstream part of the domain the flow exhibits disjoint eddies and a transfer-jet caused by the asymmetry of the roll speeds. Since there is no net transfer of liquid from roll to roll, the liquid in the transfer-jet originates in the upper inlet film. As ζ is reduced, however, liquid is also drawn from the lower inlet film (Figure 11b) and at a particular value, the interior saddle point connects to the upstream free surface. At this and smaller ζ all the liquid in the transfer-jet comes from the lower inlet film.

As ζ is decreased further, resulting in a reduction in the flow rate through the nip, the menisci move closer together and additional eddies arise (figure 11*e* and *g*) which eventually become connected together as seen in Figure 11(*h*). This flow structure marks the onset of what was earlier called the 'primary transfer-jet' for, as ζ decreases, the top saddle point disconnects from the other two and produces a long transfer-jet winding though the bead and passing between the top saddle point and the upper roll – see Figure 11(*i*). The two lower saddles then approach each other as ζ decreases and coalesce on $x = 0$. At this stage (Figure 11*j*) the upper saddle point still lies on a streamline which originates in the lower inlet film and liquid is free to pass on either side of it on the journey to the top roll. Hence there are three transfer-jets: the primary one just described, the 'secondary' one passing along the upstream free surface, and the original jet due to the unequal roll speeds.

At a smaller value of ζ the upper saddle point connects to the downstream free surface, and closes off what remains of the asymmetric-speed jet. The final change in structure occurs when the upper saddle point disconnects from the downstream free surface to form a figure-of-eight separatrix. At this value of λ no further qualitative changes are seen as $\zeta \to 0$; the primary transfer-jet grows in strength while the secondary diminishes, but the latter does not disappear. Gaskell *et al.* [10] showed that in the SFF forward roll nip, the critical flow rate at which the secondary transfer-jet disappears is given by

$$\lambda_s = \frac{2}{9}\left[\frac{3 + 2S - 2\sqrt{S^2 + 3S}}{1 + S}\right], \tag{4.8}$$

which, for $S = 2$, gives a value of 0.05. Clearly, with an inlet flux of $\lambda = 0.25$ the secondary transfer-jet will always be present, even if ζ is reduced to zero.

The case of a slower upper roll is not considered here. The flow structures can be inferred from Figure 5 by allowing for a transfer of liquid from the lower inlet to the upper outlet. For more detail the reader is referred to the extensive discussion of SFF meniscus roll coating by Summers *et al.* [14], which includes several control space diagrams and a systematic catalogue of the various possible flow structures.

5 Summary

The steady flow in a double-film-fed fluid bead has been studied using lubrication theory and finite element analysis. The size of the returning film was specified in terms of a fraction of the corresponding output film. This is a simple way of providing feedback from the output to the input of the problem and a convenient means of simulating different conditions in the gap subsequent to the one in question. The lubrication model relied on the approximation of the menisci as arcs of circles in order to obtain the capillary pressure at each end of the bead, with the simplest expression used for the radii of the arcs. Even so, good agreement was obtained between lubrication theory and finite element predictions of the film thicknesses.

The numerical solutions revealed many different flow structures which were illustrated above by means of several examples. It was seen that in the 'zero-flux' case (i.e. when $\zeta = 1$ and there is no net transfer between the rolls) the flow structure at low flow rate resembles closely that in an idealized cavity model of the flow [8]. At slightly higher flow

rates, however, the structure becomes much more intricate, featuring numerous stagnation points and recirculations. When $\zeta < 1$ liquid has to be transferred from the lower to the upper roll, and this is achieved by various meandering 'routes' or 'transfer-jets' defined by the separatrices of several saddle points.

The lubrication model was used to calculate several critical flow rates at which saddle points connect to each other and to the free surfaces, hence transforming the flow structure, and it was shown that when the total dimensionless flow rate through the bead exceeds 1/3, the downstream flow structure is independent of the relative sizes of the ingoing films. This flow rate – as in SFF roll coating – marks the distinction between the so-called 'meniscus' and 'moderately-starved' operating regimes [10].

In Part 2, the lubrication model is refined and used to explore the stability of the bead as speed ratio is increased.

Acknowledgements

The authors thank Dr J. L. Summers for useful discussions. M. C. T. Wilson is also grateful to the EPSRC for provision of a studentship.

References

[1] Benjamin, D. F. (1994) Roll coating flows and multiple roll systems. *PhD thesis*, University of Minnesota.

[2] Benjamin, D. F., Anderson, T. J. & Scriven, L. E. (1995) Multiple roll systems: steady-state operation. *AIChE J.* **41**(5), 1045–1060.

[3] Birkhoff, G. & Hays, D. F. (1963) Free boundaries in partial lubrication. *J. Math. Phys. (M.I.T.)*, **42**(2), 126–138.

[4] Bretherton, F. P. (1961) The motion of long bubbles in tubes. *J. Fluid Mech.* **10**, 166–188.

[5] Coyle, D. J. (1997) Knife and roll coating. In: S. F. Kistler and P. M. Schweizer (eds.), *Liquid Film Coating*. Chapman & Hall, pp. 539–571.

[6] Coyle, D. J., Macosko, C. W. & Scriven, L. E. (1986) Film-splitting flows in forward roll coating. *J. Fluid Mech.* **171**, 183–207.

[7] Decré, M., Gailly, E. & Buchlin, J. M. (1995) Meniscus shape experiments in forward roll coating. *Phys. Fluids*, **7**(3), 458–467.

[8] Gaskell, P. H., Gürcan, F., Savage, M. D., & Thompson, H. M. (1998) Stokes flow in a double-lid-driven cavity with free surface side-walls. *Proc. Instn. Mech. Engrs.* Part C. *J. Eng. Sci.* **212**, 387–403.

[9] Gürcan, F., Gaskell, P. H., Savage, M. D. & Wilson, M. (2000) Eddy genesis and transformation of Stokes flow in a double-lid-driven cavity. *Phys. Fluids*. Submitted.

[10] Gaskell, P. H., Savage, M. D., Summers, J. L. & Thompson, H. M. (1995) Modelling and analysis of meniscus roll coating. *J. Fluid Mech.* **298**, 113–137.

[11] Hood, P. (1976) Frontal solution program for unsymmetric matrices. *Int. J. Num. Meth. Eng.* **10**, 379–399.

[12] Kistler, S. F. & Scriven, L. E. (1983) Coating flows. In: J. R. A. Pearson and S. M. Richardson (eds.), *Computational Analysis of Polymer Processing*. Applied Science, pp. 243–299.

[13] Landau, L. & Levich, B. (1942) Dragging of a liquid by a moving plate. *Acta Physicochimica U.R.S.S.* **XVII**(1–2), 42–54.

[14] Summers, J. L., Gaskell, P. H., Savage, M. D. & Thompson, H. M. (2000) Transfer jets, flow structures and transformations in Stokes flow between contra-rotating cylinders. In preparation.

[15] Wicks, P. J., Decré, M., Planquart, Ph. & Buchlin, J. M. (1995) Flow topology associated with disjoint eddies in an asymmetric film-splitting problem. *Phys. Rev. E*, **52**(2), R1281–R1284.

[16] Wilson, M. (1997) Free surface flows between co-rotating and contra-rotating cylinders. *PhD Thesis*, University of Leeds.